Nearly degenerate $p_x + ip_y$ and $d_{x^2-y^2}$ pairing symmetry in the heavy fermion superconductor $YbRh_2Si_2$

Yu Li,[1] Qianqian Wang,[1,2] Yuanji Xu,[1,3] Wenhui Xie,[2] and Yi-feng Yang[1,3,4,*]

[1]*Beijing National Laboratory for Condensed Matter Physics and Institute of Physics, Chinese Academy of Sciences, Beijing 100190, China*

[2]*Department of Physics, Engineering Research Center for Nanophotonics and Advanced Instrument, East China Normal University, Shanghai 200062, China*

[3]*University of Chinese Academy of Sciences, Beijing 100049, China*

[4]*Songshan Lake Materials Laboratory, Dongguan, Guangdong 523808, China*

(Received 26 January 2019; revised manuscript received 7 August 2019; published 20 August 2019)

Recent discovery of superconductivity in $YbRh_2Si_2$ has raised particular interest in its pairing mechanism and gap symmetry. Here we propose a phenomenological theory of its superconductivity and investigate possible gap structures by solving the multiband Eliashberg equations combining realistic Fermi surfaces from first-principles calculations and a quantum critical form of magnetic pairing interactions. The resulting gap symmetry shows sensitive dependence on the in-plane propagation wave vector of the quantum critical fluctuations, suggesting that superconductivity in $YbRh_2Si_2$ is located on the border of $(p_x + ip_y)$ and $d_{x^2-y^2}$-wave solutions. This leads to two candidate phase diagrams: one has only a spin-triplet $(p_x + ip_y)$-wave superconducting phase; the other contains multiple phases with a spin-singlet $d_{x^2-y^2}$-wave state at zero field and a field-induced spin-triplet $(p_x + ip_y)$-wave state. In addition, the electron pairing is found to be dominated by the "jungle-gym" Fermi surface rather than the "doughnut"-like one, in contrast to previous thought. This requests a more elaborate and renewed understanding of the electronic properties of $YbRh_2Si_2$.

DOI: 10.1103/PhysRevB.100.085132

Recent discovery of superconductivity below 2 mK in $YbRh_2Si_2$ has doubled the total number of Yb-based heavy fermion superconductors [1]. While $YbRh_2Si_2$ has been a subject of decade-long studies due to its peculiar quantum critical properties [2–5], this latest discovery has stimulated new interest concerning the nature of its pairing symmetry. At higher temperatures, the angle-resolved photoemission spectroscopy (ARPES) has observed large Fermi surfaces of dominant f-orbital characters down to 1 K [6], implying the existence of itinerant Yb-4f electrons for superconducting pairing. Indeed, it is currently believed that superconductivity in $YbRh_2Si_2$ is formed of heavy-electron pairs. Still, a question remains concerning the origin of potential pairing glues and symmetry of the gap structure. A satisfactory understanding of the pairing mechanism is still lacking.

A probable candidate for the pairing glue might come from magnetic quantum critical fluctuations. Although superconductivity was so far only explored in the antiferromagnetic (AFM) phase below $T_N = 70$ mK [7], it is close to the quantum critical point due to the small critical field (0.06 T along the a-b plane and 0.66 T along the c axis) and its microscopic coexistence with AFM has been excluded [1]. The magnetically ordered phase is believed to contain significant fluctuations. It has a tiny ordered moment ($<0.1\ \mu_B/Yb^{3+}$) compared to the effective moment, $\mu_{eff} \approx 1.4\ \mu_B/Yb^{3+}$, derived from a Curie-Weiss fit of the susceptibility slightly above T_N [7,8]. Nuclear magnetic resonance has revealed strong AFM fluctuations near the quantum critical point (QCP) [9]. By contrast, neutron scattering experiments have detected significant ferromagnetic (FM) fluctuations below 30 K, which evolve into incommensurate in-plane AFM correlations with a propagation wave vector $\mathbf{Q}_\perp = \pm(0.14 \pm 0.04, 0.14 \pm 0.04)$ at 0.1 K [10]. Thus, superconductivity in $YbRh_2Si_2$ might also be mediated by magnetic quantum critical fluctuations, similar to many other heavy fermion superconductors including $CeCu_2Si_2$, $CeRhIn_5$, UGe_2, etc., in which superconductivity can also be present within a magnetic phase but mediated by spin fluctuations [11–14].

From a theoretical perspective, the phase-separated coexistence of a long-range magnetic order should play no major role in determining the superconducting gap symmetry. For simplicity, one might ignore first the presence of antiferromagnetism and consider in theory solely the superconducting instability. This allows us to calculate the pairing symmetry based on realistic heavy electron band structures derived from first-principles calculations and a phenomenological form of magnetic quantum critical pairing interactions. We find that $YbRh_2Si_2$ is located on the border of a $d_{x^2-y^2}$-wave spin-singlet state and a $(p_x + ip_y)$-wave spin-triplet state. The exact ground state depends sensitively on the in-plane (h) component of the vector $\mathbf{Q} \equiv (h, h, l)$ of the pairing interactions. This yields two candidate scenarios: one with spin-triplet $(p_x + ip_y)$-wave pairing, and the other with a spin-singlet $d_{x^2-y^2}$-wave state at zero field and an induced spin-triplet $(p_x + ip_y)$-wave state at high field.

The electronic structures of $YbRh_2Si_2$ were obtained using the density functional theory (DFT) taking into consideration both the spin-orbit coupling and an effective Coulomb

*yifeng@iphy.ac.cn

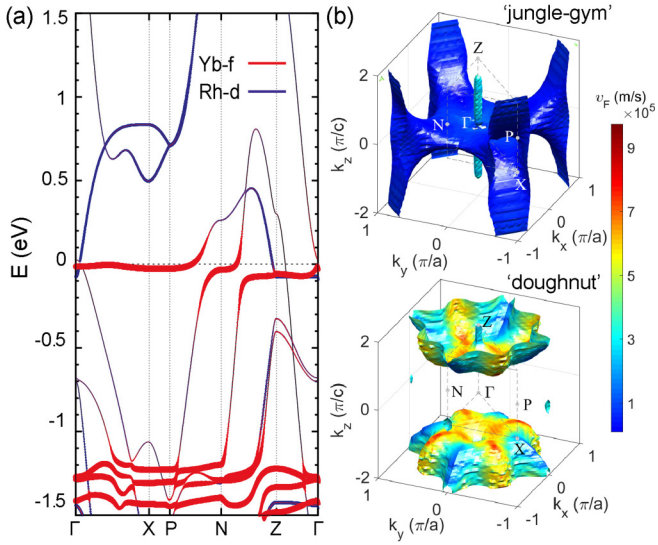

FIG. 1. (a) Electronic band structures of $YbRh_2Si_2$ from first-principles calculations, showing the f-electron character of the flat hybridization bands near the Fermi energy. (b) Illustration of the jungle-gym electron Fermi surface and the doughnutlike hole Fermi surface. The color represents the corresponding Fermi velocity, where the renormalization effect due to Z_μ is not included.

interaction $U = 8$ eV [15–18]. As shown in Fig. 1, we find two flat bands that cross the Fermi energy and exhibit strong hybridization between Yb-4f and Rh-4d orbitals. The electron band along the Γ-X-P path produces the so-called "jungle-gym" electron Fermi surface [19], and the hole band around Z point yields the "doughnut"-like hole Fermi surface. The results are plotted in Fig. 1(b) and the value of U was chosen to yield the same topological structures as in previous calculations [20,21]. Experimentally, the doughnutlike hole Fermi surface has been observed by ARPES [6,19,22–27], in agreement with theoretical predictions [20,21], while the jungle-gym electron Fermi surface was missing but argued to be covered up by surface states [6]. In de Haas–van Alphen (dHvA) measurements [28,29], a high-frequency mode has been detected and attributed to the jungle-gym Fermi surface. More detailed comparisons on the mass enhancement can be found in the Supplemental Material [30]. The agreement suggests that DFT+U provides a reasonable starting point for superconducting calculations of $YbRh_2Si_2$.

The renormalization effect of quantum critical interactions and the pairing symmetry can be investigated by solving the linearized Eliashberg equations [31–34],

$$Z_\mu(\mathbf{k}, i\omega_n) = 1 + \frac{\pi T}{\omega_n}\sum_{\nu,m}\oint_{\mathrm{FS}_\nu}\frac{d\mathbf{k}'_\parallel}{(2\pi)^3 v_{\nu,\mathbf{k}'_\mathrm{F}}}\mathrm{sgn}(\omega_m) \times V^{\mu\nu}(\mathbf{k}-\mathbf{k}', i\omega_n - i\omega_m),$$

$$\lambda\phi_\mu(\mathbf{k}, i\omega_n) = -C\pi T\sum_{\nu,m}\oint_{\mathrm{FS}_\nu}\frac{d\mathbf{k}'_\parallel}{(2\pi)^3 v_{\nu,\mathbf{k}'_\mathrm{F}}} \times \frac{V^{\mu\nu}(\mathbf{k}-\mathbf{k}', i\omega_n - i\omega_m)}{|\omega_m Z_\nu(\mathbf{k}', i\omega_m)|}\phi_\nu(\mathbf{k}', i\omega_m), \quad (1)$$

where μ and ν are the band indices, FS_ν denotes the integral over the Fermi surface of band ν, $v_{\nu,\mathbf{k}'_\mathrm{F}}$ is the corresponding Fermi velocity, $V^{\mu\nu}$ is the intraband ($\mu = \nu$) or interband ($\mu \neq \nu$) interactions, $\omega_{n/m}$ is the fermionic Matsubara frequency, Z_μ is the renormalization function, and ϕ_μ is the anomalous self-energy related to the gap function $\Delta_\mu = \phi_\mu/Z_\mu$. It is important to note that Z_μ might not only provide the major mass enhancement entering the quantum critical regime [35], but also reduces the spectral weight of pairing quasiparticles. Thus it would be incorrect to start with fully renormalized bands for superconducting calculations [30]. The prefactor C is unity for spin-singlet pairing and $-1/3$ for spin-triplet pairing. λ is the eigenvalue of the kernel matrix for each pairing channel and its largest value determines the dominant pairing state at T_c. Unlike iron-pnictides, where the Fermi surfaces are mostly quasi-two-dimensional and nearly isotropic, the Fermi surfaces here are highly anisotropic and three dimensional, so the superconducting gap structures cannot be easily captured by the low-order trigonometric harmonics near the high-symmetric points [36,37]. It is therefore necessary to derive the detailed gap structures by solving the Eliashberg equations numerically.

However, there are still two obstacles before we can proceed to do the calculations. First, controversy still remains regarding the exact form of the magnetic quantum critical fluctuations. While different theories have been proposed based on local quantum criticality [38,39] or critical quasiparticles [40–42], neutron scattering experiments seem to have detected simple spin-density-wave (SDW) type fluctuations [10]. We will not try to judge these different scenarios. Rather, we adopt a generic and phenomenological form for the pairing interactions [31–34,43,44],

$$V^{\mu\nu}(\mathbf{q}, i\nu_n) = \frac{V_0^{\mu\nu}}{1 + \xi^2(\mathbf{q}-\mathbf{Q})^2 + |\nu_n/\Lambda_{\mathrm{sf}}|^\alpha}, \quad (2)$$

where $V_0^{\mu\nu}$ are free parameters controlling the relative strength of intra- and interband pairing forces. The exponent α defines different quantum critical scenarios and takes the value of 1 for SDW [10], 0.75 for local quantum criticality [38,39], and 0.5 for critical quasiparticle theory [40–42]. We estimated the correlation length $\xi \approx 6$ Å very crudely from neutron scattering experiments [10] and chose the characteristic spin-fluctuation frequency $\Lambda_{\mathrm{sf}} \approx 1$ meV such that the magnetic Fermi energy $\Gamma_{\mathrm{sf}} = \Lambda_{\mathrm{sf}}(\xi/a)^2 \approx 2.2$ meV equals roughly the Kondo energy scale [1]. For numerical calculations, we discretize the whole Brillouin zone into $70 \times 70 \times 70$ $\mathbf{k}$ meshes and take 8192 Matsubara frequencies for the ω_n summation to be cut off at around Γ_{sf}. The gap structure in the momentum space is then solved with the approximation $g_{\mu,\mathbf{k}} \equiv \Delta_\mu(\mathbf{k}, i\omega_n) \approx \Delta_\mu(\mathbf{k}, i\pi T_c)$. Interestingly, our calculations show that the gap symmetry is independent of α but mainly determined by the momentum structure of the pairing interactions. Here comes the second obstacle that concerns $\mathbf{Q} = (h, h, l)$. Experimentally, it evolves with temperature from $h = l = 0$ (FM) below 30 K to $h = 0.14 \pm 0.04$ (AFM) at 0.1 K [10]. Since its exact value for the electron pairing at T_c is yet to be measured, we are forced to consider a wide range of possibilities around these experimental observations.

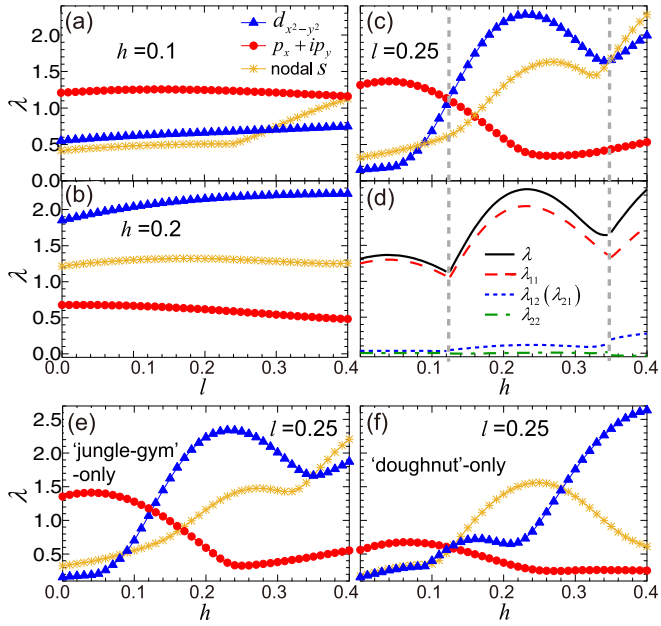

FIG. 2. Evolution of three key eigenvalues λ with varying $\mathbf{Q} = (h, h, l)$ for (a) $h = 0.1$, (b) $h = 0.2$, and (c) $l = 0.25$. (d) Band-resolved eigenvalues for the leading solution in (c) as a function of h. (e) and (f) Plot λ as a function of h with given $l = 0.25$ in the one-band calculations for each of the two Fermi surfaces. For clarity, eigenvalues that never dominate are not shown in all panels.

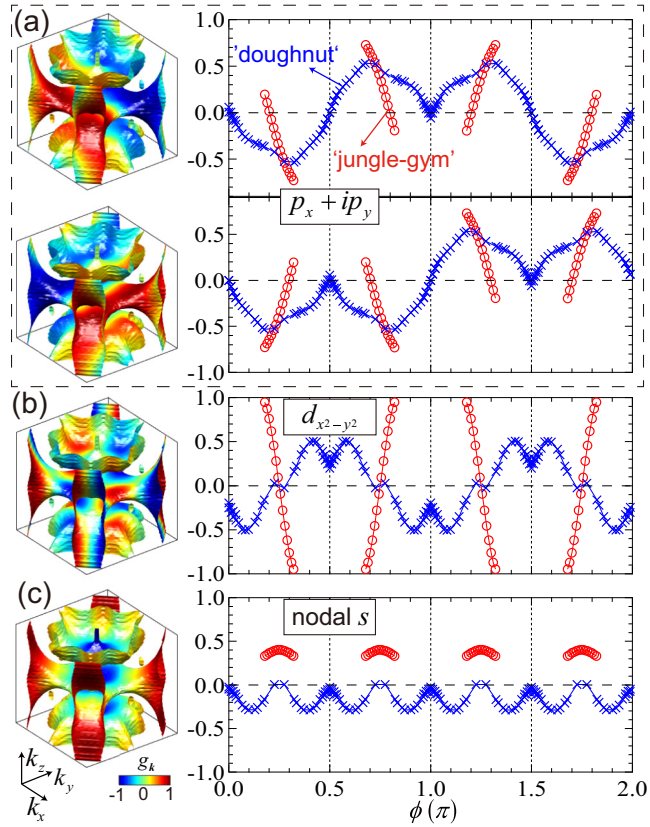

FIG. 3. Distribution of typical gap structures on the Fermi surfaces and with the azimuthal angle ϕ for (a) the p_x and p_y components of the leading $p_x + ip_y$-wave solution for $\mathbf{Q} = (0.1, 0.1, 0.25)$, (b) the leading $d_{x^2-y^2}$-wave solution for $\mathbf{Q} = (0.2, 0.2, 0.25)$, and (c) the leading nodal s-wave solution for $\mathbf{Q} = (0.4, 0.4, 0.25)$. The results are shown for $k_z = 1.5\pi/c$ plane.

Such a strategy turns out to be helpful and reveals the nearly degenerate nature of the superconductivity in $YbRh_2Si_2$.

Figure 2 plots the eigenvalues of three major pairing channels for different choices of $\mathbf{Q}$. For simplicity, we only present the data for $\alpha = 1$ and assume a band-independent $V_0^{\mu\nu}$. We have examined other choices in a reasonable range of variations and found no qualitative influence on our main conclusions (see the Supplemental Material [30]). Figures 2(a) and 2(b) compare the eigenvalues as a function of l for fixed $h = 0.1$ and 0.2, revealing a leading solution of either $(p_x + ip_y)$ or $d_{x^2-y^2}$-wave over a wide parameter range of l. Thus the electron pairing is insensitive to magnetic fluctuations along c axis. We also plot the h dependence of the eigenvalues for a typical $l = 0.25$ in Fig. 2(c), where we could see clear transitions of the leading pairing channel from $(p_x + ip_y)$ to $d_{x^2-y^2}$ at $h \approx 0.13$ and then to a nodal s-wave solution at $h \approx 0.35$, indicating that in-plane magnetic fluctuations play a crucial role in determining the pairing symmetry. For clarity, typical gap structures of above solutions are plotted in Fig. 3 for different values of h at fixed $l = 0.25$. For $h = 0.1$, we derive a twofold degenerate solution with p_x and p_y symmetry as shown in their dependence on the azimuthal angle (ϕ). Their mixture gives the chiral $(p_x + ip_y)$-wave gap to minimize the pairing energy $E = -\frac{1}{3}\sum_{\substack{\mathbf{k},\mathbf{k}',\mu,\\ \nu,\alpha,\beta}} V^{\mu\nu}_{\mathbf{k}\mathbf{k}'}\langle c^\dagger_{\mu,\mathbf{k}\alpha} c^\dagger_{\mu,-\mathbf{k}\beta}\rangle\langle c_{\nu,-\mathbf{k}'\beta} c_{\nu,\mathbf{k}'\alpha}\rangle$, where α and β are spin indices. For $h = 0.2$, a $d_{x^2-y^2}$-wave gap is obtained which changes sign when ϕ rotates by $\pi/2$ and contains nodes on the $k_x = \pm k_y$ plane. For $h = 0.4$, we identify a nodal s-wave solution with accidental nodes on the doughnutlike Fermi surface.

To extract key factors that determine the pairing symmetry, we separate out contributions from each Fermi surface and define the band-resolved eigenvalues [45],

$$\lambda_{\mu\nu} = \frac{\oint_{\mathrm{FS}_\mu} \frac{d\mathbf{k}_\parallel}{(2\pi)^3 v_{\mu,\mathbf{k}_\mathrm{F}}} \oint_{\mathrm{FS}_\nu} \frac{d\mathbf{k}'_\parallel}{(2\pi)^3 v_{\nu,\mathbf{k}'_\mathrm{F}}} K^{\mu\nu}_{\mathbf{k},\mathbf{k}'} g^*_{\mu,\mathbf{k}} g_{\nu,\mathbf{k}'}}{\oint_{\mathrm{FS}_\mu} \frac{d\mathbf{k}_\parallel}{(2\pi)^3 v_{\mu,\mathbf{k}_\mathrm{F}}} |g_{\mu,\mathbf{k}}|^2}, \quad (3)$$

where $K^{\mu\nu}_{\mathbf{k},\mathbf{k}'} = -C\pi T_c \sum_m V^{\mu\nu}_{\mathbf{k},\mathbf{k}'}(i\pi T_c - i\omega_m)/|\omega_m|$ and $V^{\mu\nu}_{\mathbf{k},\mathbf{k}'}(i\nu_n) = [V^{\mu\nu}(\mathbf{k}-\mathbf{k}', i\nu_n) \pm V^{\mu\nu}(\mathbf{k}+\mathbf{k}', i\nu_n)]/2$ for spin-singlet (+) and triplet (−) pairings, respectively. $\lambda_{\mu\nu}$ represents the effective pairing strength between the μ and ν Fermi surfaces. For $\mu = \nu$, it denotes the intraband contribution within each Fermi surface, while for $\mu \neq \nu$, it accounts for the contribution from interband pair scattering. The true eigenvalue is a sum of all terms, $\lambda = \sum_{\mu,\nu} \lambda_{\mu\nu}$. Figure 2(d) plots the band-resolved $\lambda_{\mu\nu}$ for the leading solutions in each regime as a function of h. In all three regimes, λ_{11} is always the largest, implying that the jungle-gym electron Fermi surface is the major player in forming superconductivity. To understand this, we consider the electron pairing on each single Fermi surface alone and solve the one band Eliashberg equations with the same parameters. The results are compared in Figs. 2(e) and 2(f). For small h, both Fermi surfaces have the same leading

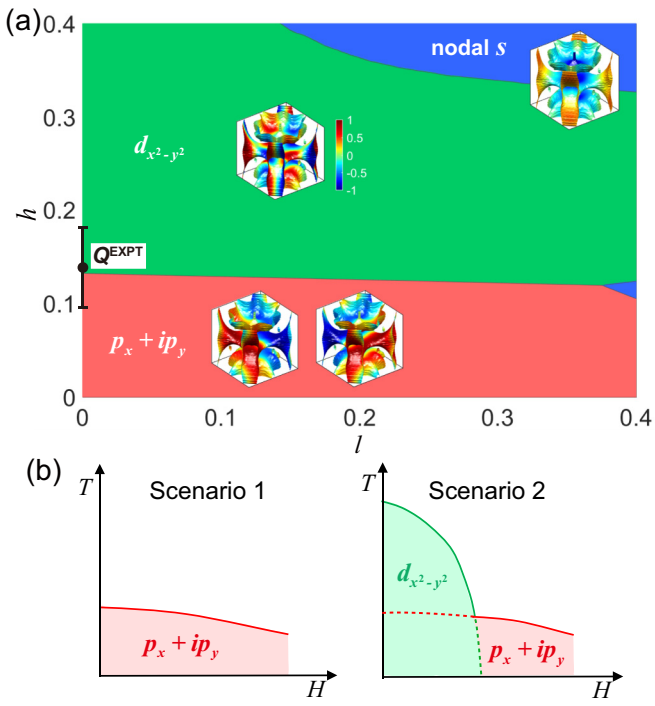

FIG. 4. (a) Theoretical phase diagram of the superconductivity in $YbRh_2Si_2$ as a function of the propagation wave vector $\mathbf{Q} = (h, h, l)$ of pairing interactions. The insets illustrate the gap structures in each phase. $\mathbf{Q}^{\mathrm{EXPT}} = (0.14, 0.14, 0)$ marks the observed $\mathbf{Q}$ in neutron scattering experiments at 0.1 K. The error bar represents the experimental error $h = 0.14 \pm 0.04$. (b) Two candidate T-H phase diagrams of the superconductivity with dominant $(p_x + ip_y)$ or $d_{x^2-y^2}$-wave solutions at zero magnetic field.

$(p_x + ip_y)$-wave solution owing to the ferromagneticlike pairing interaction; while for intermediate h, the jungle-gym Fermi surface favors a $d_{x^2-y^2}$-wave gap but the doughnutlike Fermi surface yields a nodal s-wave gap. Thus for the two-band model, the jungle-gym Fermi surface dominates the leading pairing channel and gives rise to the $d_{x^2-y^2}$-wave gap for intermediate h. We attribute this to the special topology of the jungle-gym Fermi surface which is more strongly nested and matches better the momentum structure of the pairing glue than the doughnutlike one (see the Supplemental Material for an illustration of their respective nesting properties [30]). The fact that λ_{22} is suppressed to almost zero in the two-band calculations compared to its value in the single-band calculations reflects microscopic competition of the pair formation on two Fermi surfaces. We would like to note that the doughnutlike Fermi surface was often treated as the major or only player in previous literature. Our results suggest that this might be an oversimplified picture.

Figure 4 summarizes all the leading solutions on a global phase diagram of the superconductivity with varying $\mathbf{Q}$ for $YbRh_2Si_2$. Among them, $(p_x + ip_y)$ dominates the lower part of the phase diagram with small h, $d_{x^2-y^2}$ governing most of the upper part, while the nodal s-wave solution only occurs at the corners. These are not unexpected, as the $(p_x + ip_y)$-wave solution is a spin-triplet state favored by FM-like fluctuations with small h, $d_{x^2-y^2}$ originating from the nested jungle-gym Fermi surface and associated AFM fluctuations, and the nodal s-wave solution, which is not crucial, might appear when large-momentum transfers start to correlate Cooper pairs on different portions of the Fermi surfaces. The true ground state of the superconductivity in $YbRh_2Si_2$ can then be determined if the exact wave vector responsible for the pairing below T_c are known. Unfortunately, this requires a very challenging experiment which so far has not yet been done. For candidate $\mathbf{Q}^{\mathrm{EXPT}} = (0.14, 0.14, 0)$ measured by neutron scattering at 0.1 K above the AFM order [10], a $d_{x^2-y^2}$-wave gap is obtained but located very close to the $d_{x^2-y^2}$ and $(p_x + ip_y)$ phase boundary. A slight variation due to experimental error $(h = 0.14 \pm 0.04)$ would lead to a spin-triplet $(p_x + ip_y)$-wave pairing. Further uncertainty may arise from a potential temperature evolution of the $\mathbf{Q}$ vector. Very recently, it was also proposed in the critical quasiparticle theory that additional energy fluctuations might favor a p-wave solution [46]. Thus, a natural statement would be that the superconductivity in $YbRh_2Si_2$ is located in a delicate position with nearly degenerate $d_{x^2-y^2}$ and $(p_x + ip_y)$-wave symmetries. It is easy to imagine that a magnetic field would presumably shift the balance and promote the $(p_x + ip_y)$-wave spin-triplet solution. We thus speculate two possible scenarios for the T-H (temperature-magnetic field) phase diagrams as sketched schematically in Fig. 4(b). If the $(p_x + ip_y)$-wave spin-triplet state wins out, there would only be a single superconducting phase under a field. By contrast, if the $d_{x^2-y^2}$-wave spin-singlet state is stronger, it might be more rapidly suppressed by an external magnetic field and the $(p_x + ip_y)$-wave spin-triplet state could then be induced, causing multiple superconducting phases.

Yet experiments so far are inconclusive. In the original work, only one superconducting phase was reported below about 2 mK [1]. It has an extrapolated upper critical field $H_{c2}(T \to 0) \approx 30$–$50$ mT, comparable to its orbital limiting field $H_{c2,\mathrm{orb}} = 0.693(-dH_{c2}/dT)|_{T_c} T_c \approx 35$ mT [47], but well beyond the Pauli limiting field $H_{c2,\mathrm{P}} = 1.84 T_c \approx 3.7$ mT [48,49]. Since the Pauli limit is generally associated with pair breaking of the spin singlet, the fact that $H_{c2,\mathrm{P}} \ll H_{c2,\mathrm{orb}} \approx H_{c2}$ manifests dominant orbital effects and suggests that this single superconducting phase should be of spin-triplet pairing, in agreement with the first scenario in Fig. 4(b). However, the latest experiment reported a different zero-field superconducting phase with $T_c \approx 6$ mK and its transition to a field-induced phase with $T_c \approx 2$ mK at about 4 mT [50], pointing towards the possibility of multiple superconducting phases tuned by the magnetic field. The two phases show very different field dependence of T_c. While the field-induced phase is very similar to the originally observed (spin-triplet) one [1], the zero-field phase has an extrapolated upper critical field $H_{c2}(T \to 0) \approx 4$ mT, which is below its Pauli limiting field $H_{c2,\mathrm{P}} = 1.84 T_c \approx 11$ mT. Since $H_{c2} < H_{c2,\mathrm{P}}$, the zero-field phase is most probably spin singlet. Thus the latest experiment seems to support the second scenario proposed in Fig. 4(b). If this is the case, our theory predicts that the zero-field phase should be a $d_{x^2-y^2}$-wave spin-singlet state, and the field-induced phase would then be a $(p_x + ip_y)$-wave spin-triplet state. This implies the existence of multiple superconducting phases is an intrinsic electronic property of $YbRh_2Si_2$,

although the presence of nuclear order might play a role in the phase diagram. The seeming "inconsistency" of two experiments, possibly influenced by some yet-to-be-identified factors in the experimental setup, might actually be a supporting evidence for our proposal of two nearly degenerate pairing states.

To summarize, we have proposed a quantum critical pairing mechanism for the newly discovered superconductivity in $YbRh_2Si_2$ and explored its possible gap symmetry using phenomenological pairing interactions with realistic band structures from first-principles calculations. For proper experimental parameters, we obtain nearly degenerate $d_{x^2-y^2}$ and $(p_x + ip_y)$-wave solutions. This leads to two candidate temperature-magnetic field phase diagrams. While the original experiment seems to support a single $(p_x + ip_y)$-wave superconducting phase, the latest experiment supports the scenario of two superconducting phases. In the latter case, our result implies a spin-singlet $d_{x^2-y^2}$-wave pairing state at zero field and a field-induced spin-triplet $(p_x + ip_y)$-wave state. Our calculations show that the jungle-gym Fermi surface plays the major role for electron pairing rather than the doughnutlike one. This differs from the conventional picture and requests more elaborate investigations in pursuit of a concrete and thorough understanding of the electronic properties of $YbRh_2Si_2$.

This work was supported by the National Natural Science Foundation of China (NSFC Grants No. 11774401, No. 11522435, and No. 51572086), the National Key R&D Program of China (Grant No. 2017YFA0303103), and the Youth Innovation Promotion Association of CAS.

[1] E. Schuberth, M. Tippmann, L. Steinke, S. Lausberg, A. Steppke, M. Brando, C. Krellner, C. Geibel, R. Yu, Q. Si, and F. Steglich, Science **351**, 485 (2016).
[2] J. Custers, P. Gegenwart, H. Wilhelm, K. Neumaier, Y. Tokiwa, O. Trovarelli, C. Geibel, F. Steglich, C. Pépin, and P. Coleman, Nature (London) **424**, 524 (2003).
[3] S. Paschen, T. Lühmann, S. Wirth, P. Gegenwart, O. Trovarelli, C. Geibel, F. Steglich, P. Coleman, and Q. Si, Nature (London) **432**, 881 (2004).
[4] S. Friedemann, T. Westerkamp, M. Brando, N. Oeschler, S. Wirth, P. Gegenwart, C. Krellner, C. Geibel, and F. Steglich, Nat. Phys. **5**, 465 (2009).
[5] O. Stockert and F. Steglich, Annu. Rev. Condens. Matter Phys. **2**, 79 (2011).
[6] K. Kummer, S. Patil, A. Chikina, M. Güttler, M. Höppner, A. Generalov, S. Danzenbächer, S. Seiro, A. Hannaske, C. Krellner, Y. Kucherenko, M. Shi, M. Radovic, E. Rienks, G. Zwicknagl, K. Matho, J. W. Allen, C. Laubschat, C. Geibel, and D. V. Vyalikh, Phys. Rev. X **5**, 011028 (2015).
[7] O. Trovarelli, C. Geibel, S. Mederle, C. Langhammer, F. M. Grosche, P. Gegenwart, M. Lang, G. Sparn, and F. Steglich, Phys. Rev. Lett. **85**, 626 (2000).
[8] P. Gegenwart, J. Custers, C. Geibel, K. Neumaier, T. Tayama, K. Tenya, O. Trovarelli, and F. Steglich, Phys. Rev. Lett. **89**, 056402 (2002).
[9] K. Ishida, K. Okamoto, Y. Kawasaki, Y. Kitaoka, O. Trovarelli, C. Geibel, and F. Steglich, Phys. Rev. Lett. **89**, 107202 (2002).
[10] C. Stock, C. Broholm, F. Demmel, J. Van Duijn, J. W. Taylor, H. J. Kang, R. Hu, and C. Petrovic, Phys. Rev. Lett. **109**, 127201 (2012).
[11] C. Pfleiderer, Rev. Mod. Phys. **81**, 1551 (2009).
[12] B. D. White, J. D. Thompson, and M. B. Maple, Physica C **514**, 246 (2015).
[13] D. J. Scalapino, Rev. Mod. Phys. **84**, 1383 (2012).
[14] Y.-F. Yang, D. Pines, and N. J. Curro, Phys. Rev. B **92**, 195131 (2015).
[15] J. P. Perdew, K. Burke, and M. Ernzerhof, Phys. Rev. Lett. **77**, 3865 (1996).
[16] V. I. Anisimov, F. Aryasetiawan, and A. Lichtenstein, J. Phys.: Condens. Matter **9**, 767 (1997).
[17] M.-T. Suzuki and H. Harima, J. Phys. Soc. Jpn. **79**, 024705 (2010).
[18] P. Blaha, K. Schwarz, G. K. H. Madsen, D. Kvasnicka, and J. Luitz, *Wien2k: An Augmented Plane Wave Plus Local orbital Program for Calculating the Crystal Properties* (Technical University of Wien, Austria, 2018).
[19] G. A. Wigger, F. Baumberger, Z.-X. Shen, Z. P. Yin, W. E. Pickett, S. Maquilon, and Z. Fisk, Phys. Rev. B **76**, 035106 (2007).
[20] S. Friedemann, S. Wirth, N. Oeschler, C. Krellner, C. Geibel, F. Steglich, S. MaQuilon, Z. Fisk, S. Paschen, and G. Zwicknagl, Phys. Rev. B **82**, 035103 (2010).
[21] G. Zwicknagl, Rep. Prog. Phys. **79**, 124501 (2016).
[22] D. V. Vyalikh, S. Danzenbächer, A. N. Yaresko, M. Holder, Y. Kucherenko, C. Laubschat, C. Krellner, Z. Hossain, C. Geibel, M. Shi, L. Patthey, and S. L. Molodtsov, Phys. Rev. Lett. **100**, 056402 (2008).
[23] D. V. Vyalikh, S. Danzenbächer, Y. Kucherenko, C. Krellner, C. Geibel, C. Laubschat, M. Shi, L. Patthey, R. Follath, and S. L. Molodtsov, Phys. Rev. Lett. **103**, 137601 (2009).
[24] D. V. Vyalikh, S. Danzenbächer, Y. Kucherenko, K. Kummer, C. Krellner, C. Geibel, M. G. Holder, T. K. Kim, C. Laubschat, M. Shi, L. Patthey, R. Follath, and S. L. Molodtsov, Phys. Rev. Lett. **105**, 237601 (2010).
[25] S. Danzenbächer, D. V. Vyalikh, K. Kummer, C. Krellner, M. Holder, M. Höppner, Y. Kucherenko, C. Geibel, M. Shi, L. Patthey, S. L. Molodtsov, and C. Laubschat, Phys. Rev. Lett. **107**, 267601 (2011).
[26] S.-K. Mo, W. S. Lee, F. Schmitt, Y. L. Chen, D. H. Lu, C. Capan, D. J. Kim, Z. Fisk, C.-Q. Zhang, Z. Hussain, and Z.-X. Shen, Phys. Rev. B **85**, 241103(R) (2012).
[27] K. Kummer, D. V. Vyalikh, L. Rettig, R. Cortés, Y. Kucherenko, C. Krellner, C. Geibel, U. Bovensiepen, M. Wolf, and S. L. Molodtsov, Phys. Rev. B **86**, 085139 (2012).
[28] P. M. C. Rourke, A. McCollam, G. Lapertot, G. Knebel, J. Flouguet, and S. R. Julian, Phys. Rev. Lett. **101**, 237205 (2008).
[29] A. Sutton, P. Rourke, V. Taufour, A. McCollam, G. Lapertot, G. Knebel, J. Flouquet, and S. Julian, Phys. Status Solidi (b) **247**, 549 (2010).
[30] See Supplemental Material at http://link.aps.org/supplemental/10.1103/PhysRevB.100.085132 for additional details and calculations.
[31] Y.-F. Yang and D. Pines, Proc. Natl. Acad. Sci. USA **111**, 18178 (2014).

[32] Y. Li, M. Liu, Z. Fu, X. Chen, F. Yang, and Y.-F. Yang, Phys. Rev. Lett. **120**, 217001 (2018).
[33] P. Monthoux and D. Pines, Phys. Rev. Lett. **69**, 961 (1992).
[34] S. Nishiyama, K. Miyake, and C. M. Varma, Phys. Rev. B **88**, 014510 (2013).
[35] P. Gegenwart, Y. Tokiwa, T. Westerkamp, F. Weickert, J. Custers, J. Ferstl, C. Krellner, C. Geibel, P. Kerschl, K.-H. Mülller, and F. Steglich, New J. Phys. **8**, 171 (2006).
[36] S. Maiti, M. M. Korshunov, T. A. Maier, P. J. Hirschfeld, and A. V. Chubukov, Phys. Rev. Lett. **107**, 147002 (2011).
[37] A. Chubukv, Annu. Rev. Condens. Matter Phys. **3**, 57 (2012).
[38] Q. Si, S. Rabello, K. Ingersent, and J. L. Smith, Nature (London) **413**, 804 (2001).
[39] Q. Si, J. H. Pixley, E. Nica, S. J. Yamamoto, P. Goswami, R. Yu, and S. Kirchner, J. Phys. Soc. Jpn. **83**, 061005 (2014).
[40] P. Wölfle and E. Abrahams, Phys. Rev. B **84**, 041101(R) (2011).
[41] E. Abrahams and P. Wölfle, Proc. Natl. Acad. Sci. USA **109**, 3238 (2012).
[42] P. Wölfle, J. Schmalian, and E. Abrahams, Rep. Prog. Phys. **80**, 044501 (2017).
[43] A. J. Millis, H. Monien, and D. Pines, Phys. Rev. B **42**, 167 (1990).
[44] P. Monthoux, A. V. Balatsky, and D. Pines, Phys. Rev. Lett. **67**, 3448 (1991).
[45] T. A. Maier, S. Graser, D. J. Scalapino, and P. J. Hirschfeld, Phys. Rev. B **79**, 224510 (2009).
[46] J. Kang, R. M. Fernandes, E. Abrahams, and P. Wölfle, Phys. Rev. B **98**, 214515 (2018).
[47] N. R. Werthamer, E. Helfand, and P. C. Hohenberg, Phys. Rev. **147**, 295 (1966).
[48] A. M. Clogston, Phys. Rev. Lett. **9**, 266 (1962).
[49] B. S. Chandrasekhar, Appl. Phys. Lett. **1**, 7 (1962).
[50] J. Saunders, Quantum materials into the microkelvin regime (Advanced School and Workshop on Correlations in Electron Systems: from Quantum Criticality to Topology, 2018), http://indico.ictp.it/event/8330/session/39/contribution/106; J. Saunders, Superconductivity in $YbRh_2Si_2$: electrical transport and noise experiments (12th International Conference on Materials and Mechanisms of Superconductivity and High Temperature Superconductors, 2018).